Arxiv: 2404.01926

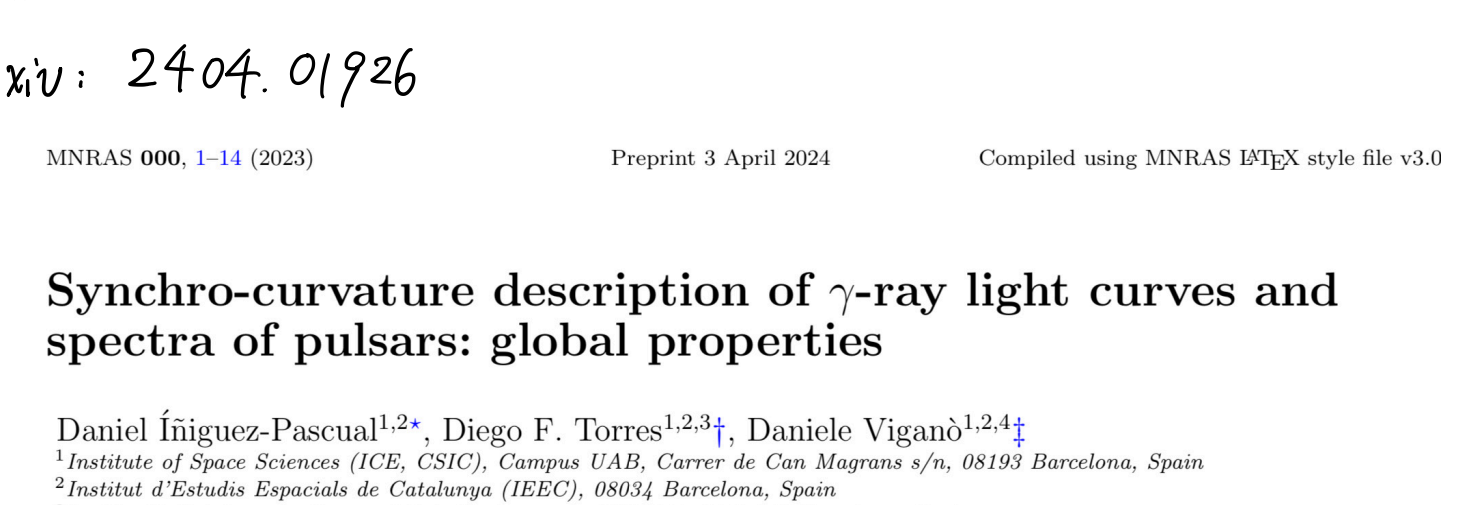

MNRAS 000, 1–14 (2023) Preprint 3 April 2024 Compiled using MNRAS LaTeX style file v3.0

Synchro-curvature description of γ-ray light curves and spectra of pulsars: global properties

Daniel Íñiguez-Pascual[1,2*], Diego F. Torres[1,2,3†], Daniele Viganò[1,2,4‡]
[1] Institute of Space Sciences (ICE, CSIC), Campus UAB, Carrer de Can Magrans s/n, 08193 Barcelona, Spain
[2] Institut d'Estudis Espacials de Catalunya (IEEC), 08034 Barcelona, Spain
[3] Institució Catalana de Recerca i Estudis Avançats (ICREA), E-08010 Barcelona, Spain
[4] Institute of Applied Computing & Community Code (IAC3), University of the Balearic Islands, Palma, 07122, Spain

(accepted for pulication in MNRAS)

1. Intro:

Accelerating regions:

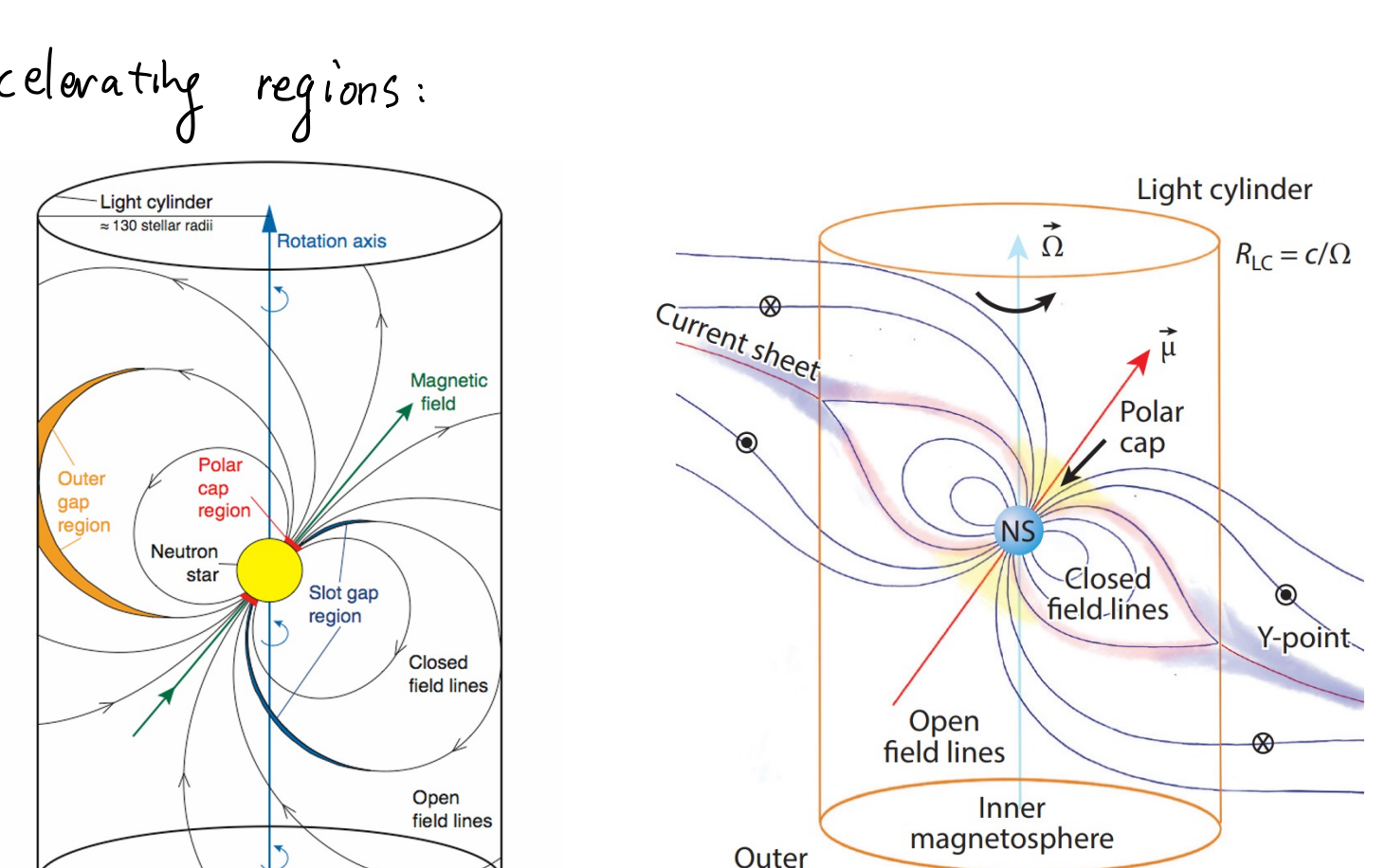

The MAGIC collaboration 2008 (Kramer & Philippov 2022)

Within light cylinder: { Polar Gap
Slot Gap
Outer Gap

$\rho \neq \rho_{GJ}$ locally ⬇ $E_{//}$

Near light cylinder: Y-point

Out of light cylinder: current sheet

Question: relating models with observation?

Hard to fully calculate radiation from 1st principle models ... PIC simulation...

⇒ This paper: geometrically present emission position.

➕

Synchro-Curvature radiation

2. Radiative & Geometrical modeling

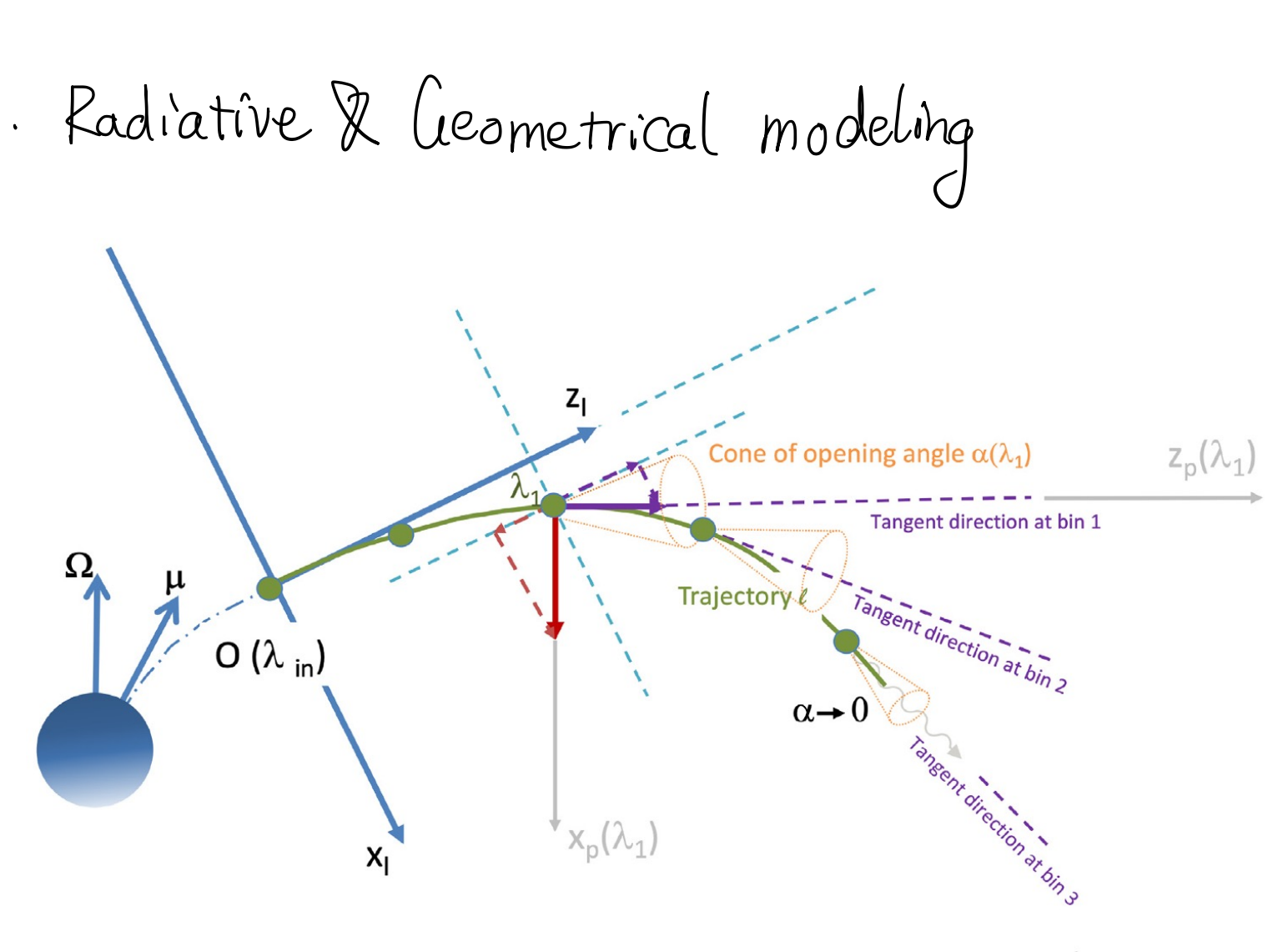
z_l
Cone of opening angle $\alpha(\lambda_1)$
$z_p(\lambda_1)$
λ_1
Tangent direction at bin 1
Trajectory
Tangent direction at bin 2
Tangent direction at bin 3
$\alpha \to 0$
Ω
μ
$O(\lambda_{in})$
x_l
$x_p(\lambda_1)$
Normal vector at λ_1
Normal vector components [0,1]
Tangent vector at λ_1
Tangent vector components [0,1]

Viganò & Torres 2019

λ: coordinates along the rotating magnetic field ("gyro-averaged trajectory")

particle's motion: $E_{//}$ v.s. radiation loss

$\Uparrow$

Γ: Lorentz factor
α: pinch angle
B: local magnetic field
r_c: curvature radius

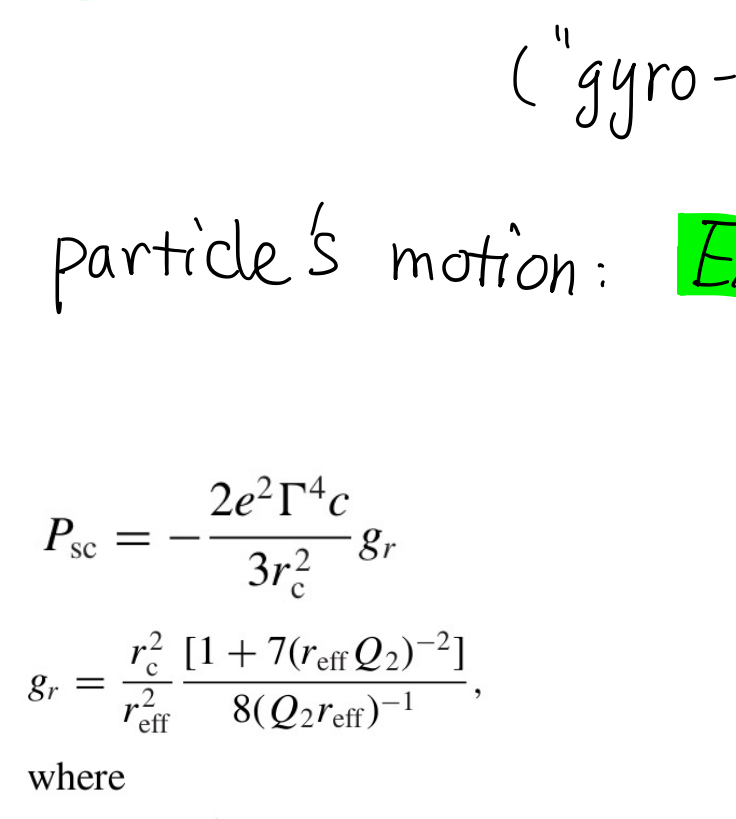

$$P_{sc} = -\frac{2e^2\Gamma^4 c}{3r_c^2} g_r$$

$$g_r = \frac{r_c^2}{r_{eff}^2}\frac{[1+7(r_{eff}Q_2)^{-2}]}{8(Q_2 r_{eff})^{-1}},$$

where

$$Q_2^2 = \frac{\cos^4\alpha}{r_c^2}\left[1+3\xi+\xi^2+\frac{r_{gyr}}{r_c}\right],$$

$$r_{eff} = \frac{r_c}{\cos^2\alpha}\left(1+\xi+\frac{r_{gyr}}{r_c}\right)^{-1},$$

$$r_{gyr} = \frac{\Gamma v_\perp mc}{eB} = \frac{\Gamma\beta\sin\alpha mc^2}{eB},$$

$$\xi = \frac{r_c}{r_{gyr}}\frac{\sin^2\alpha}{\cos^2\alpha} \simeq 5.9\times10^3\frac{r_{c,8}B_6\sin\alpha}{\Gamma_7\cos^2\alpha}.$$

Viganò et al. 2015 (a)

$$B = B_s\cdot\left(\frac{R_s}{x_{in}R_{lc}+\lambda}\right)^b$$

$$r_c = R_{lc}\sqrt{x_{in}R_{lc}+\frac{\lambda}{R_{lc}}}$$

x_{in}: injection points (acceleration region) 1~1.5 R_{LC}

⇛ yields α & Γ

⇛ spectral distribution

When it comes to γ-rays, $\Gamma\sim10^7$, $\alpha\downarrow\downarrow$ (almost slides along magnetic field lines)

- description of particle's motion:

Frenet-Serret formulae

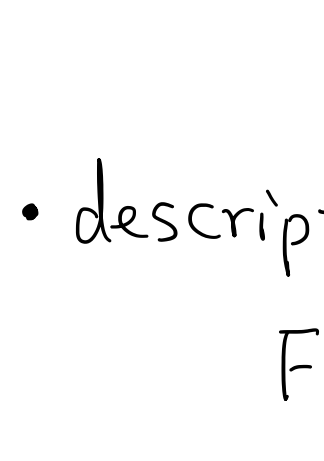

$$\frac{d\hat{t}}{d\lambda} = \frac{1}{r_c}\hat{n},$$

$$\frac{d\hat{n}}{d\lambda} = -\frac{1}{r_c}\hat{t}+\tau\hat{b},$$

$$\frac{d\hat{b}}{d\lambda} = -\tau\hat{n}.$$

$\hat{t}$: tangential
$\hat{n}$: normal
$\hat{b} = \hat{t}\times\hat{n}$ binormal
τ: torsion

$\tau(\lambda) = \frac{1}{r_c(\lambda)}$ torsion ~ curvature

- emission direction: $\Gamma^{-1}\sim10^{-6}\sim10^{-7}\ll1$

= α + χ (gyro)

emission direction = $(\alpha(\lambda), \chi)$
= moving direction
$dD(\lambda)/d\Omega_\Omega$

actual coordinate: $(\theta_{obs}, \phi_\Omega)$
↓ LOS ↓ pulsar rotational phase

- emission location & emission region's shape

dipole magnetic field { incline angle = Ψ_Ω
magnetic colatitude = Ψ_μ

based on some qualitative description given by former theoretical studies (Bogovalov 1999, Tchekhovskoy et al. 2016)

Centres of emission region:

$$\Psi_\mu^c(\xi_\mu, R, \Psi_\Omega) = \frac{\pi}{2} + A(R,\Psi_\Omega)\sin(\xi_\mu - \frac{\pi}{2})$$

$$[A(R,\Psi_\Omega) = K\,\Psi_\Omega(R/R_{LC} - R^0/R_{LC})^2]$$

emission region extends: $[\Psi_\mu^c - \Delta\Psi_\mu/2,\ \Psi_\mu^c + \Delta\Psi_\mu/2]$

- energy spectrum: integrate trajectory from start to end.

$$\frac{dP_{tot}}{dE} = \int_{\lambda_{in}}^{\lambda_{out}}\left\langle\frac{dP_{sc}(\lambda)}{dE}\right\rangle\frac{dN(\lambda)}{d\lambda}d\lambda$$

particle distribution: $\frac{dN}{d\lambda} = \frac{N_0}{x_0}\cdot\frac{e^{-\frac{\lambda-\lambda_{in}}{x_0}}}{1-e^{-\frac{\lambda_{out}-\lambda_{in}}{x_0}}}$

▲ emission map (photon flux / dE / dΩ)

$$M_E(\theta_{obs}, \phi_\Omega, E) = \int_{R^0}^{R^0+\Delta R}\int_{\lambda_{in}}^{\lambda_{out}}\int_0^{2\pi}\int_{\Delta\Psi_\mu}\frac{dD(\lambda)}{d\Omega_\Omega}\left\langle\frac{dP_{sc}(\lambda)}{dE}\right\rangle\frac{dN(\lambda)}{d\lambda}d\Psi_\mu d\xi_\mu d\lambda dx_{in}$$

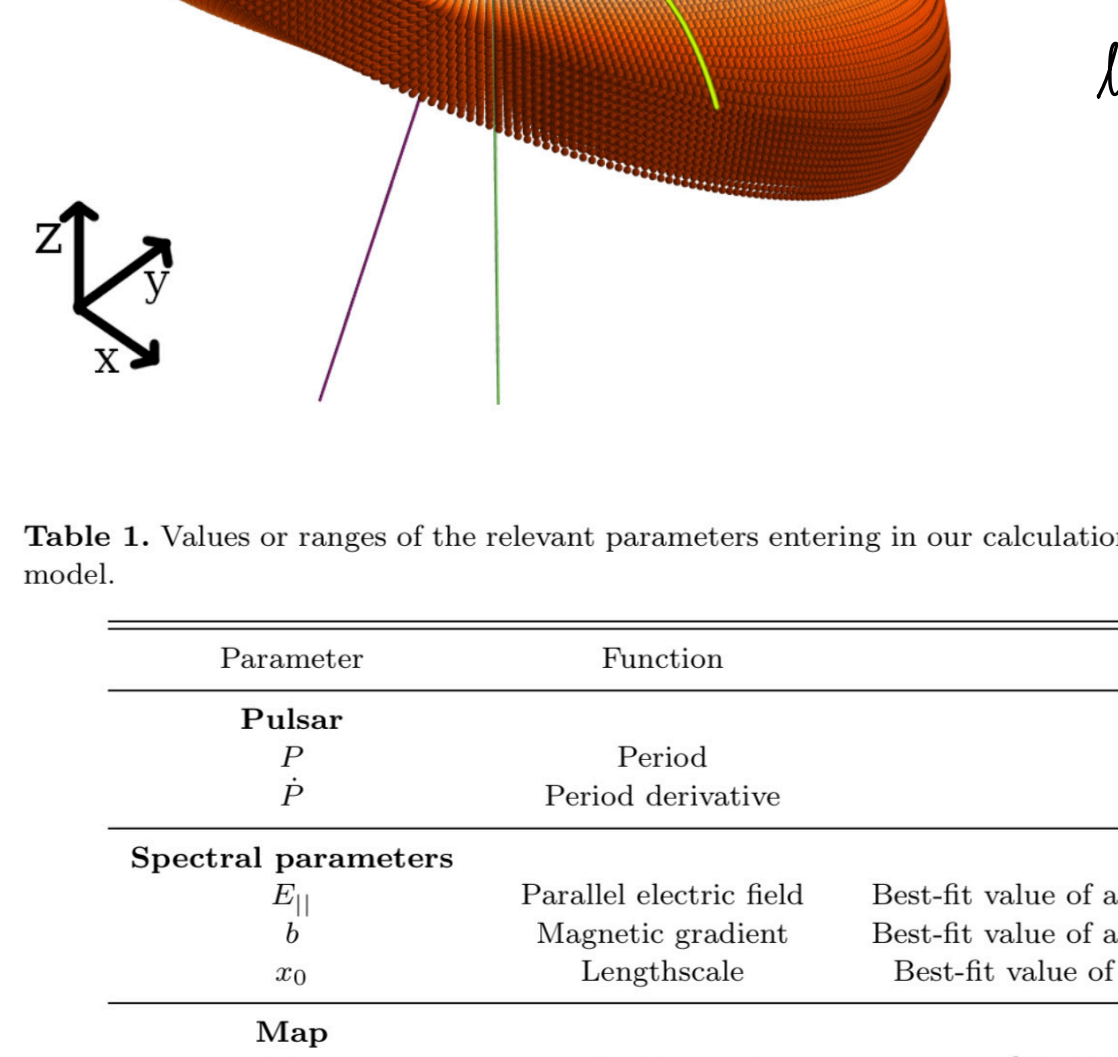

color: white → red
inner to outer

light yellow line: one of trajectories

light grey lines: R_{LC}

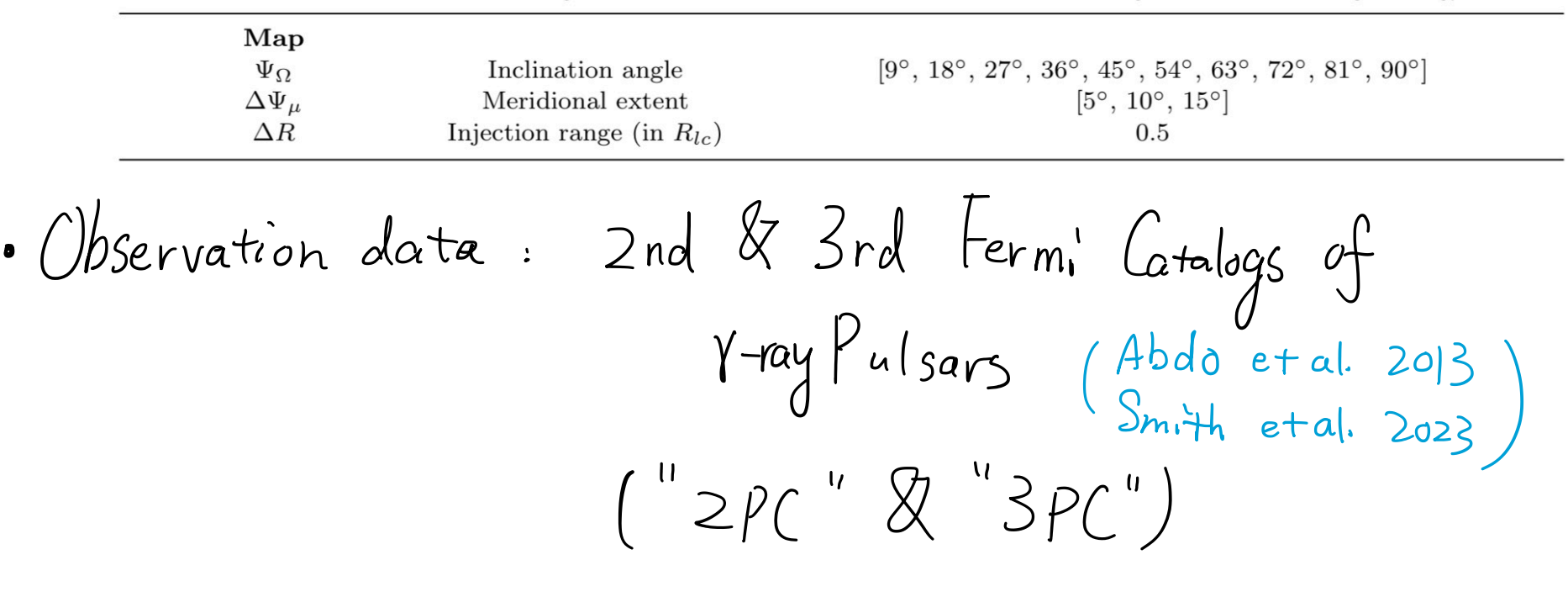

Table 1. Values or ranges of the relevant parameters entering in our calculation, together with a brief description of their function in the model.

Parameter	Function	Value/range selected
Pulsar		
P	Period	Depending on the pulsar
$\dot{P}$	Period derivative	Depending on the pulsar
Spectral parameters		
$E_{\|\|}$	Parallel electric field	Best-fit value of an spectral fitting of the pulsar's high-energy SED
b	Magnetic gradient	Best-fit value of an spectral fitting of the pulsar's high-energy SED
x_0	Lengthscale	Best-fit value of spectral fitting of the pulsar's high-energy SED
Map		
Ψ_Ω	Inclination angle	[9°, 18°, 27°, 36°, 45°, 54°, 63°, 72°, 81°, 90°]
$\Delta\Psi_\mu$	Meridional extent	[5°, 10°, 15°]
ΔR	Injection range (in R_{lc})	0.5

- Observation data: 2nd & 3rd Fermi Catalogs of γ-ray Pulsars (Abdo et al. 2013 Smith et al. 2023)

("2PC" & "3PC")

10 representative pulsars chosen

Table 2. Timing and best-fitting spectral parameters of the ten selected pulsars, The spectral model here considers 21 injection points evenly distributed from 1.0 to 1.5 R_{lc}. Last two columns show the number of peaks of the observational light curve released in the 2PC and 3PC for each pulsar.

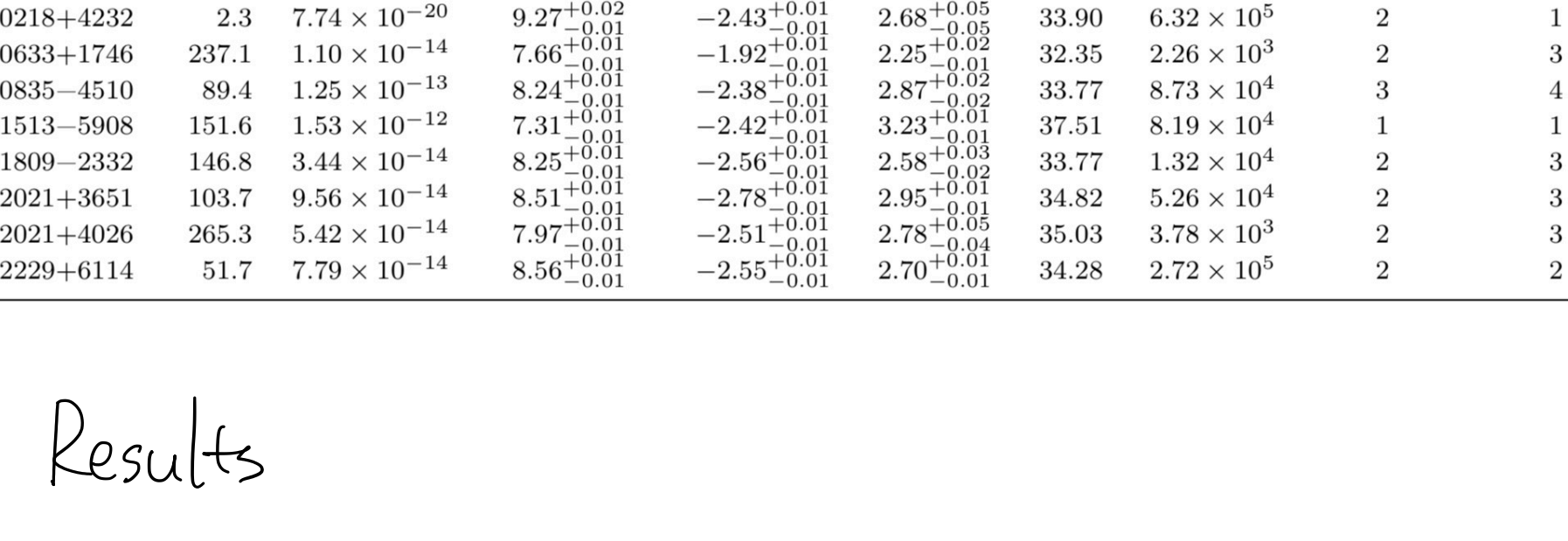

Pulsar	P [ms]	$\dot{P}$ [s/s]	$\log E_{\|\|}$ [V/m]	$\log(x_0/R_{lc})$	b	$\log N_0$	$B_{lc}^{b=3}(G)$	Peaks 2PC	Peaks 3PC
J0007+7303	315.9	3.57×10^{-13}	$8.29^{+0.01}_{-0.01}$	$-2.67^{+0.01}_{-0.01}$	$2.49^{+0.02}_{-0.02}$	33.95	6.28×10^3	2	3
J0205+6449	65.7	1.92×10^{-13}	$8.98^{+0.01}_{-0.01}$	$-3.08^{+0.01}_{-0.01}$	$2.62^{+0.02}_{-0.02}$	34.02	2.32×10^5	2	2
J0218+4232	2.3	7.74×10^{-20}	$9.27^{+0.02}_{-0.01}$	$-2.43^{+0.01}_{-0.01}$	$2.68^{+0.05}_{-0.05}$	33.90	6.32×10^5	2	1
J0633+1746	237.1	1.10×10^{-14}	$7.66^{+0.01}_{-0.01}$	$-1.92^{+0.01}_{-0.01}$	$2.25^{+0.02}_{-0.01}$	32.35	2.26×10^3	2	3
J0835−4510	89.4	1.25×10^{-13}	$8.24^{+0.01}_{-0.01}$	$-2.38^{+0.01}_{-0.01}$	$2.87^{+0.02}_{-0.02}$	33.77	8.73×10^4	3	4
J1513−5908	151.6	1.53×10^{-12}	$7.31^{+0.01}_{-0.01}$	$-2.42^{+0.01}_{-0.01}$	$3.23^{+0.01}_{-0.01}$	37.51	8.19×10^4	1	1
J1809−2332	146.8	3.44×10^{-14}	$8.25^{+0.01}_{-0.01}$	$-2.56^{+0.01}_{-0.01}$	$2.58^{+0.03}_{-0.02}$	33.77	1.32×10^4	2	3
J2021+3651	103.7	9.56×10^{-14}	$8.51^{+0.01}_{-0.01}$	$-2.78^{+0.01}_{-0.01}$	$2.95^{+0.01}_{-0.01}$	34.82	5.26×10^4	2	3
J2021+4026	265.3	5.42×10^{-14}	$7.97^{+0.01}_{-0.01}$	$-2.51^{+0.01}_{-0.01}$	$2.78^{+0.05}_{-0.04}$	35.03	3.78×10^3	2	3
J2229+6114	51.7	7.79×10^{-14}	$8.56^{+0.01}_{-0.01}$	$-2.55^{+0.01}_{-0.01}$	$2.70^{+0.01}_{-0.01}$	34.28	2.72×10^5	2	2

3. Results

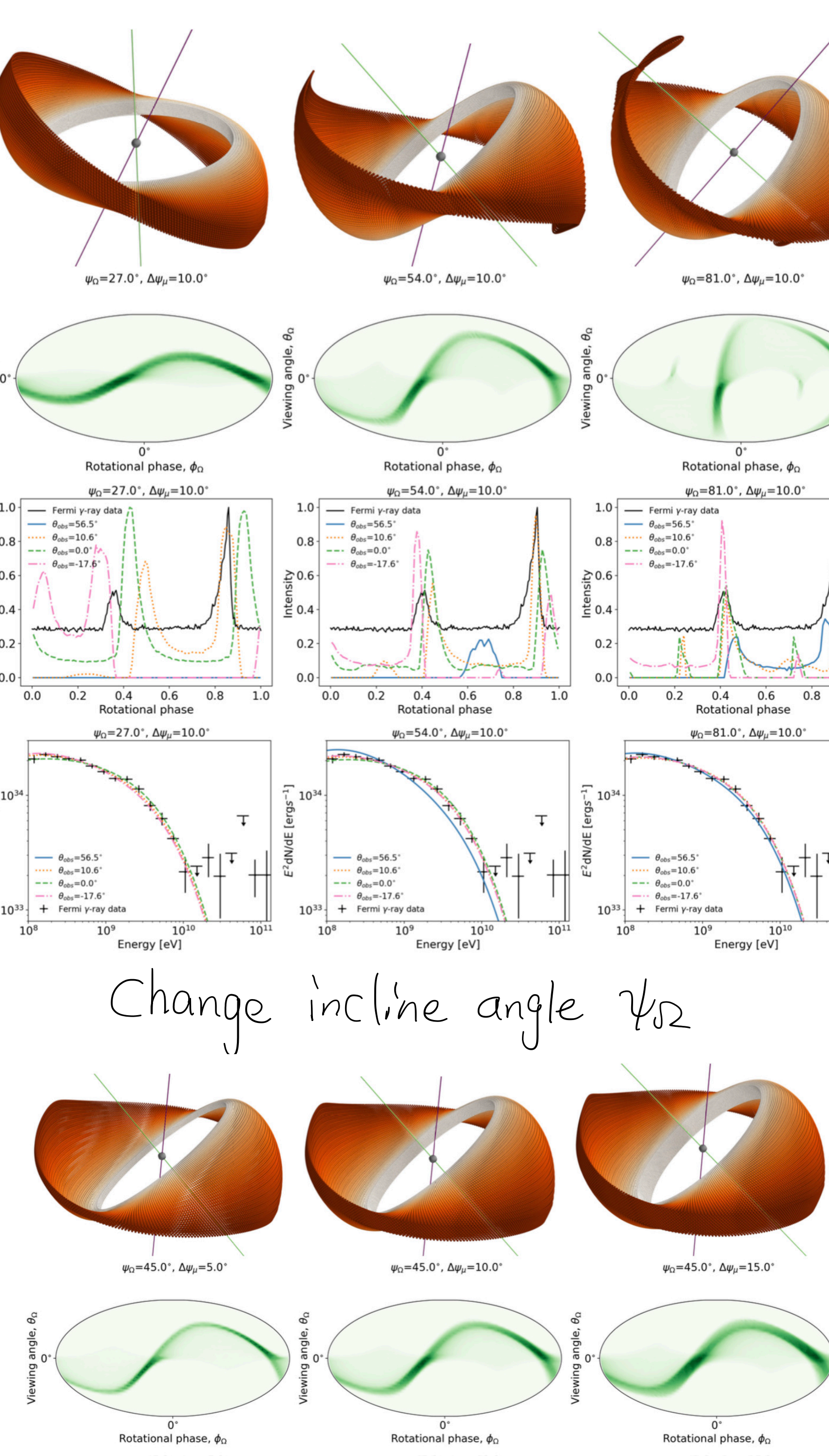

LOS varies

Change incline angle Ψ_Ω

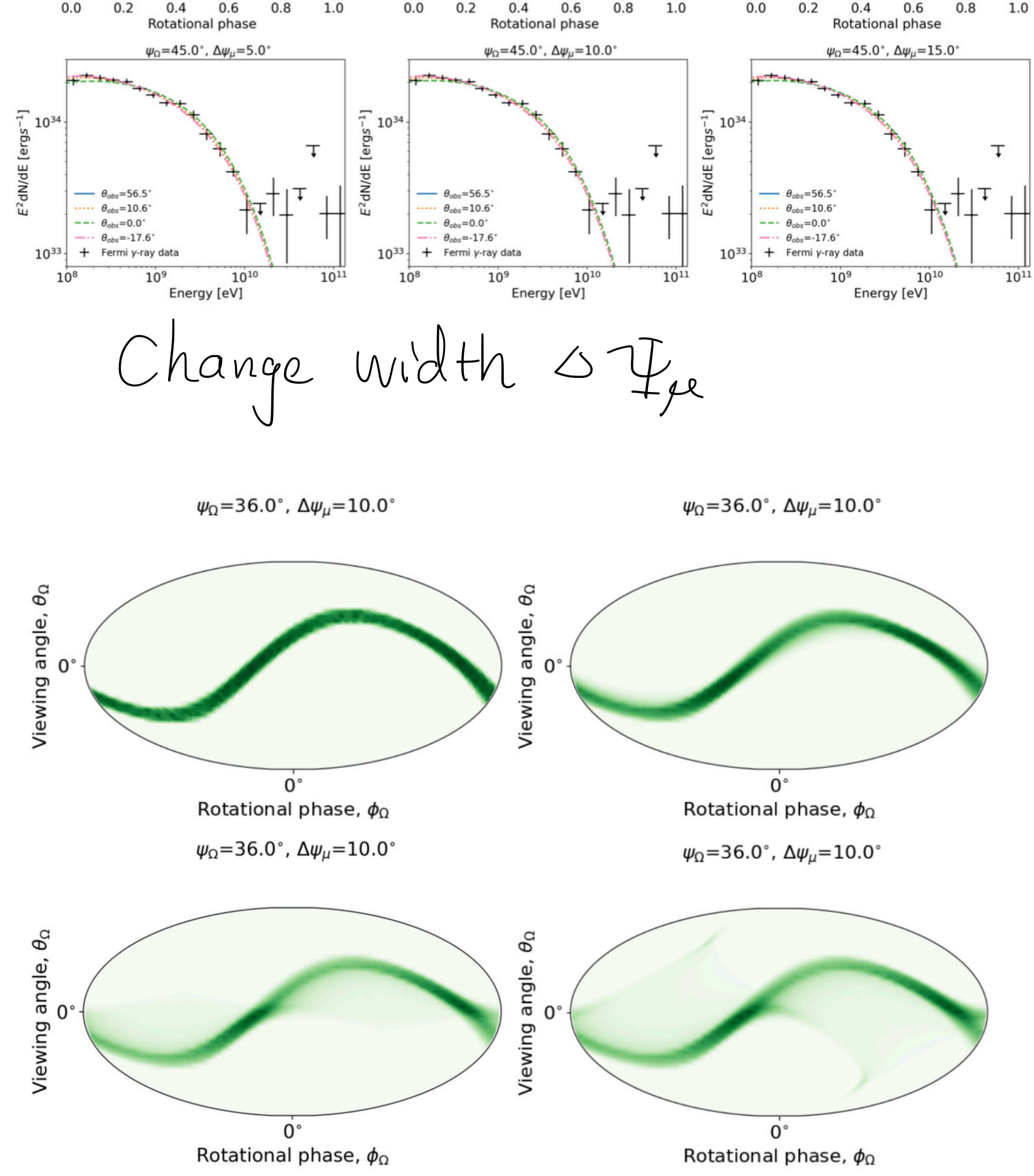

Change width $\Delta\Psi_\mu$

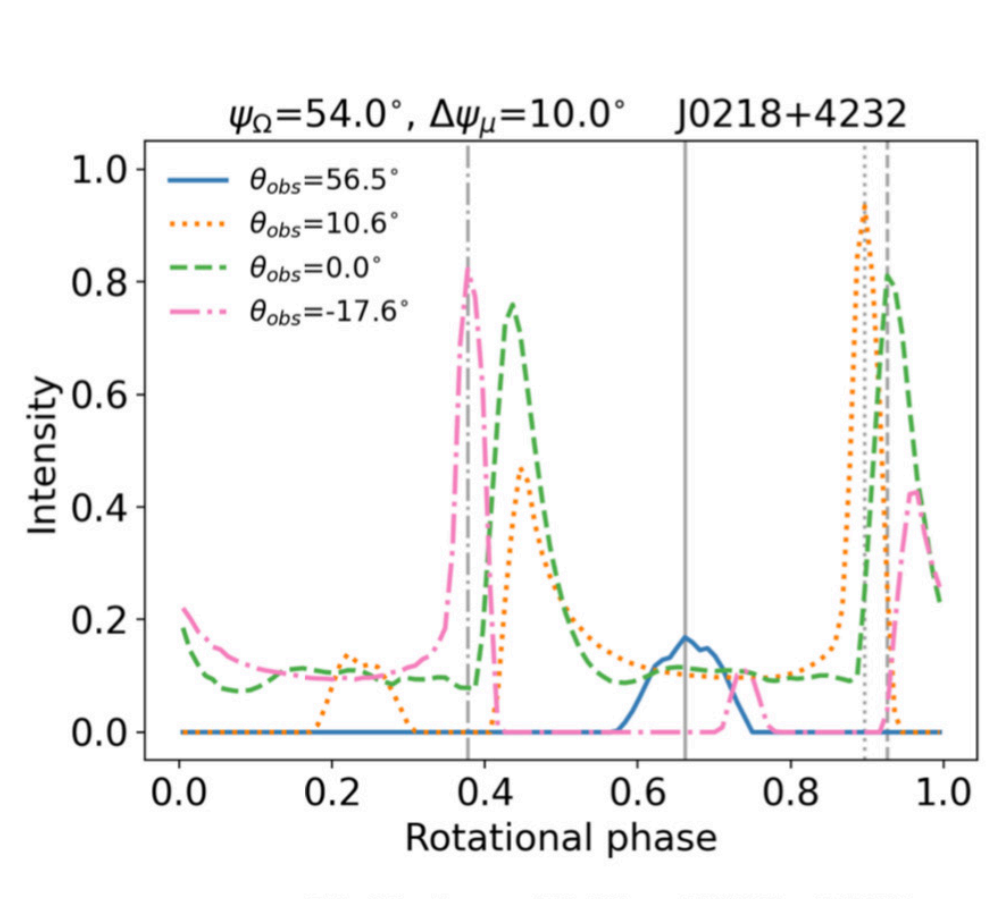

Change ΔR (injection length)

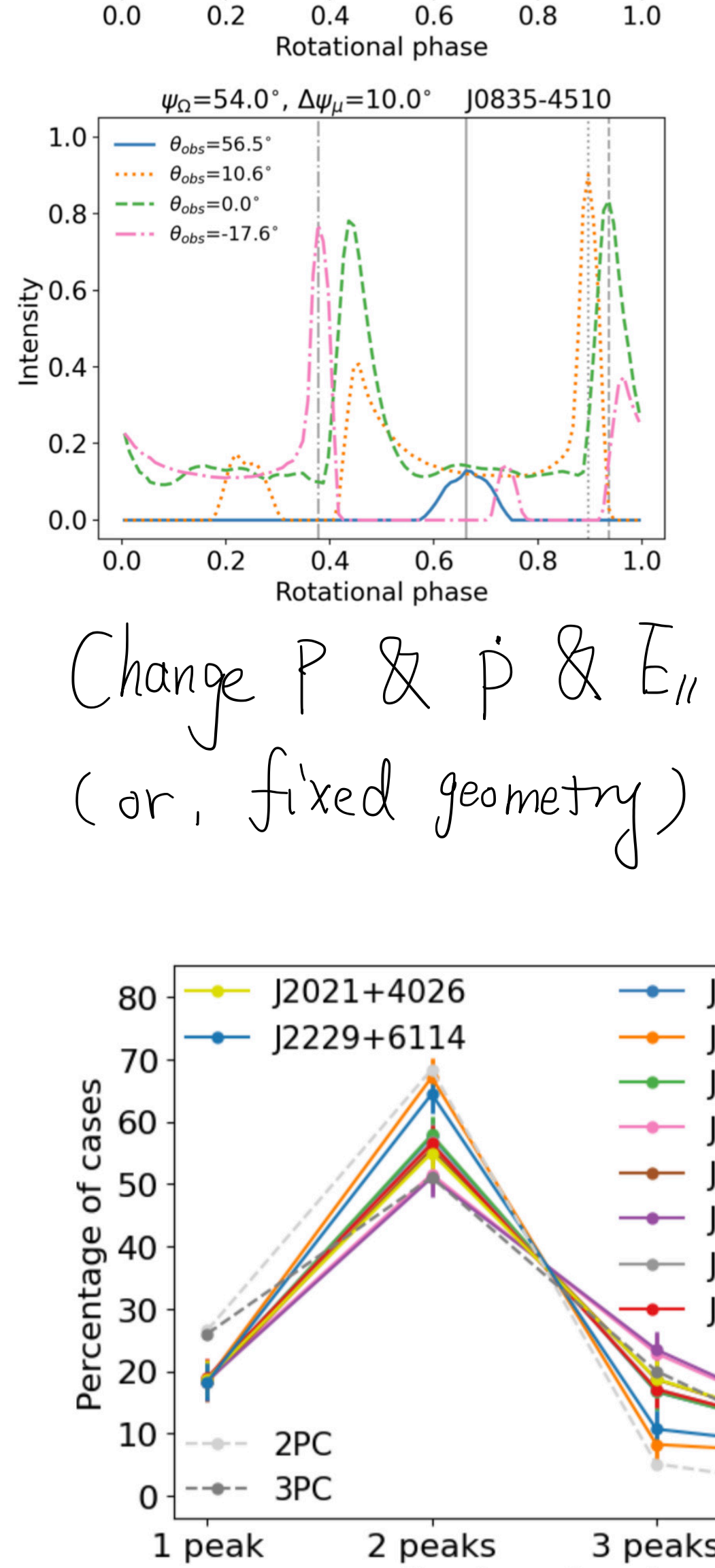

Change P & $\dot{P}$ & $E_{//}$ & b & x_0
(or, fixed geometry)

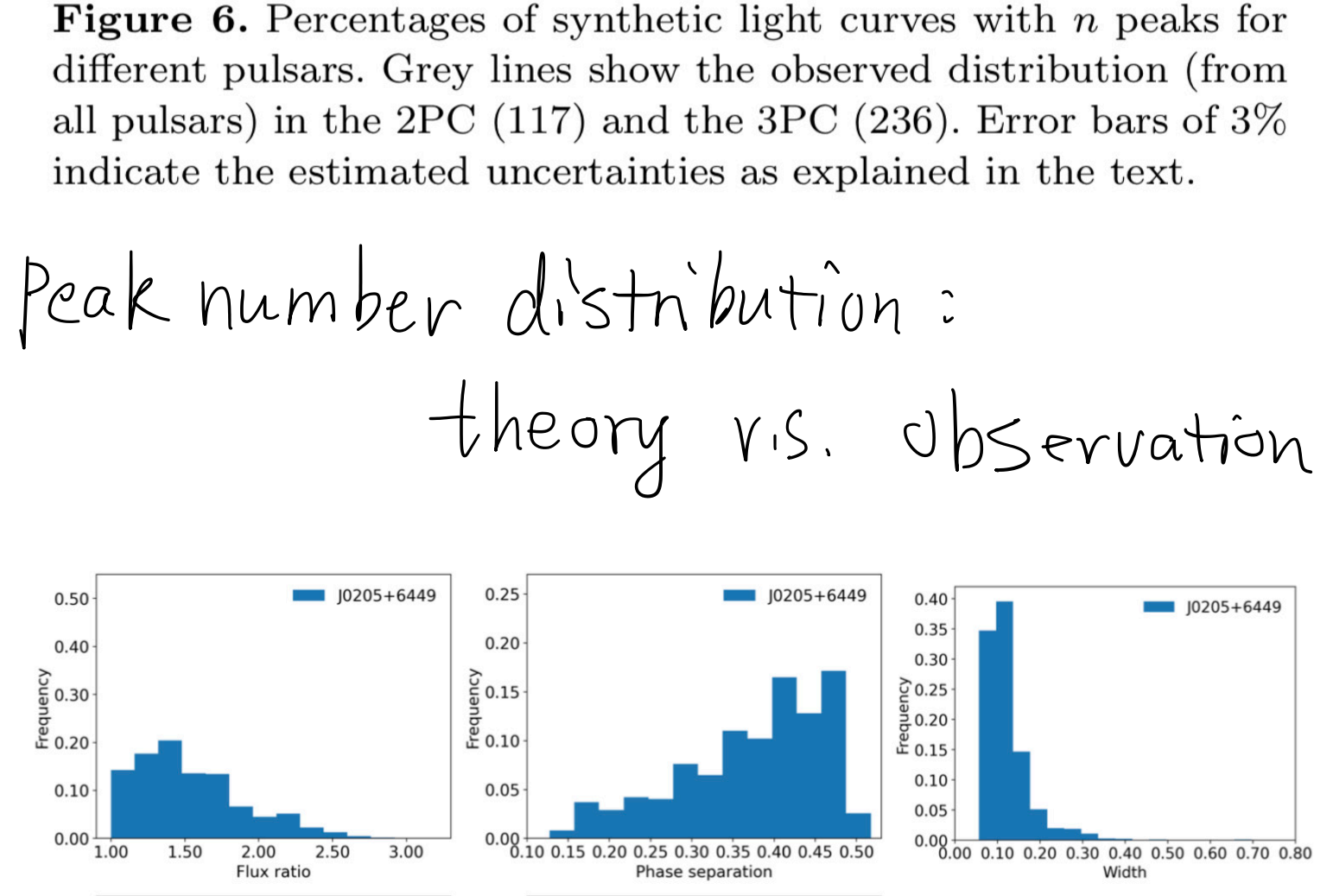

Figure 6. Percentages of synthetic light curves with n peaks for different pulsars. Grey lines show the observed distribution (from all pulsars) in the 2PC (117) and the 3PC (236). Error bars of 3% indicate the estimated uncertainties as explained in the text.

Peak number distribution:
theory v.s. observation

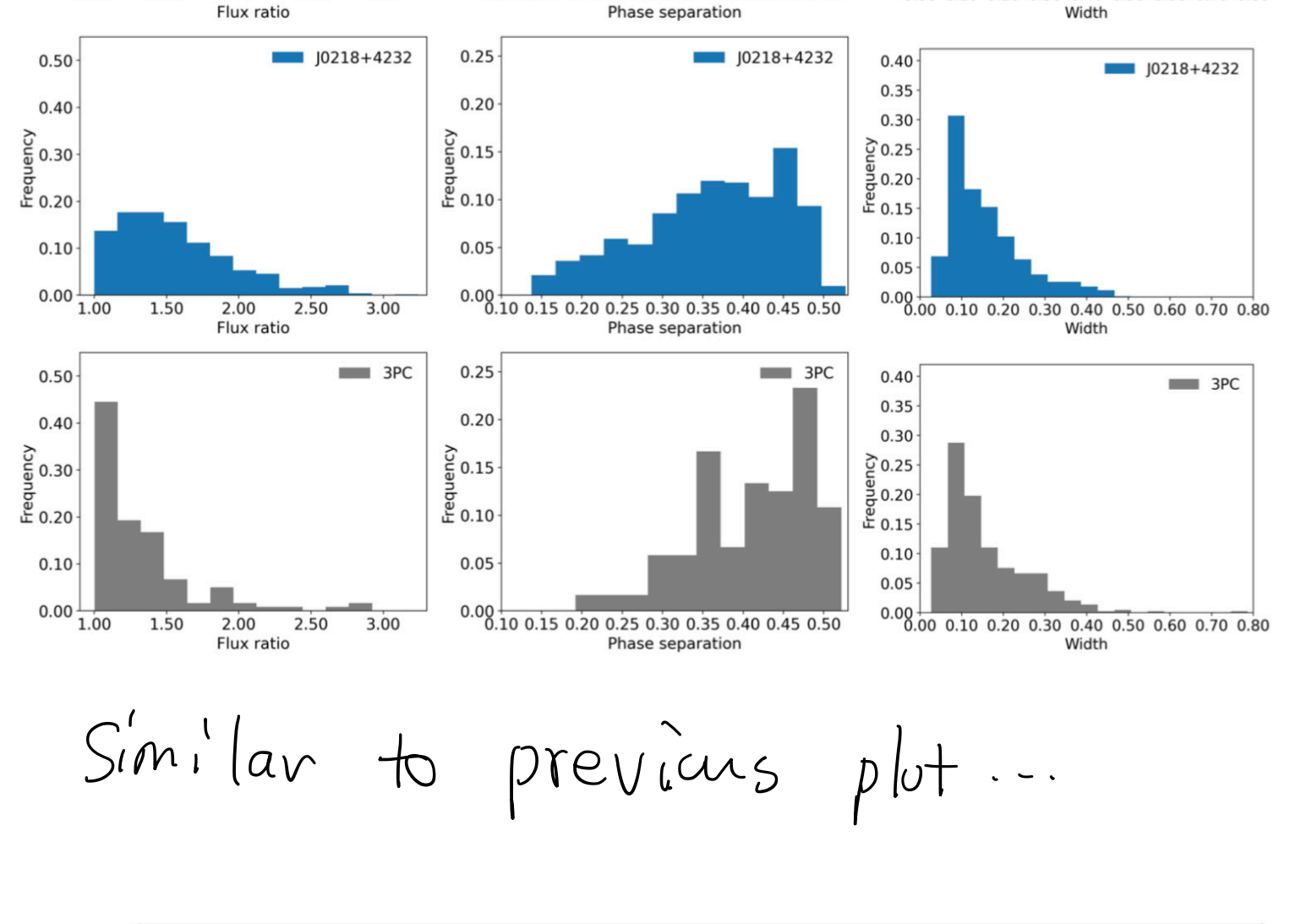

Similar to previous plot ...

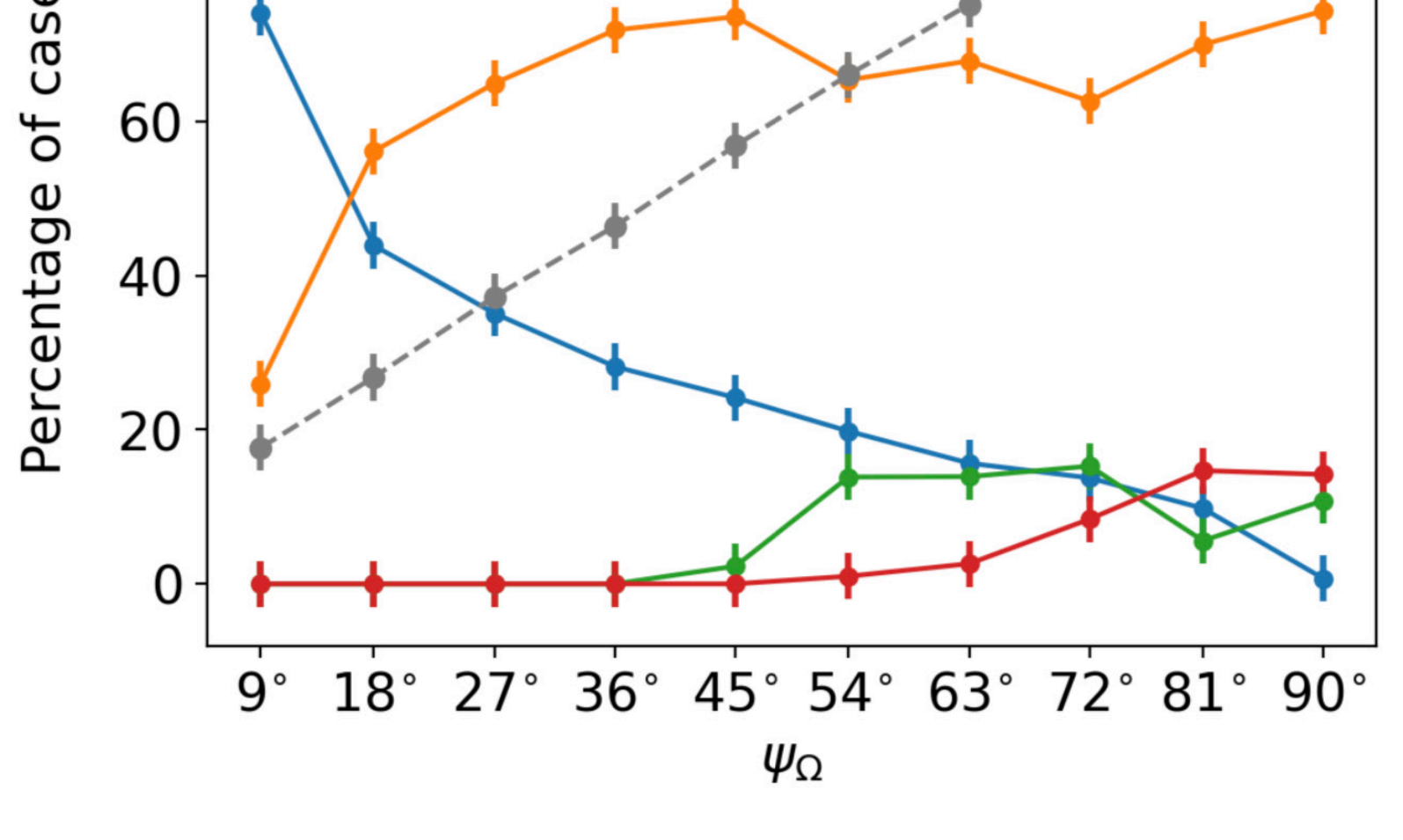

Detection rates v.s. incline angles

☆ Geometry affects observation mostly